Biogeosciences

Partitioning of carbon export in the euphotic zone of the oligotrophic South China Sea

Yifan Ma, Kuanbo Zhou, Weifang Chen, Junhui Chen, Jin-Yu Terence Yang, and Minhan Dai

State Key Laboratory of Marine Environmental Science, College of Ocean and Earth Sciences,
Xiamen University, Xiamen, 361102, China

Correspondence: Minhan Dai (mdai@xmu.edu.cn)

Abstract. We conducted samplings of total and particulate ^{234}Th, along with particulate organic carbon (POC), in the summer of 2017 to examine nutrient-dependent structures of export productivity within the euphotic zone (Ez) of the oligotrophic basin of the South China Sea (SCS). Nitrate concentrations throughout the study area were below detection limits in the nutrient-depleted layer (NDL) above the nutricline, while they sharply increased with depth in the nutrient-replete layer (NRL) across the nutricline until the base of the Ez. Based on our vertical profilings of ^{234}Th–^{238}U disequilibria, this study estimated for the first time POC export fluxes both out of the NDL and at the horizon of the Ez base. The total ^{234}Th deficit relative to ^{238}U was determined in the NDL at all study sites. By contrast, ^{234}Th was mostly in equilibrium with ^{238}U in the NRL, except at the northernmost station, SEATS (SouthEast Asian Time-series Study; 18° N, 116° E), where the ^{234}Th deficit was also observed in the NRL. By combining 1D steady-state ^{234}Th fluxes and POC/^{234}Th ratios, we derived vertical patterns of POC export fluxes. The POC export fluxes at station SEATS were $1.6 \pm 0.6 \, \text{mmol C m}^{-2} \, \text{d}^{-1}$ at the NDL base, accounting for approximately half of that at the base of the Ez. For the rest of the sampling sites, the POC export fluxes at the NDL base (averaged at $2.3 \pm 1.1 \, \text{mmol C m}^{-2} \, \text{d}^{-1}$) were comparable with those at the base of the Ez ($1.9 \pm 0.5 \, \text{mmol C m}^{-2} \, \text{d}^{-1}$), suggesting rapid export of POC out of the NDL. This finding fundamentally changes our traditional view that the NDL, being depleted in nutrients, would not be a net exporter of POC. Furthermore, our results revealed a significant positive correlation between POC export fluxes at the NDL base and the potential of subsurface nutrient supplies, indicated by nutricline depth and nutrient concentrations obtained from both in situ measurements and numerical modeling. POC export fluxes (averaged at $3.4 \pm 1.2 \, \text{mmol C m}^{-2} \, \text{d}^{-1}$) at the NDL base at stations with shallow nutriclines and high levels of subsurface nutrients approximately doubled those (averaged at $1.6 \pm 0.5 \, \text{mmol C m}^{-2} \, \text{d}^{-1}$) at other stations. We subsequently used a two-endmember mixing model based on the mass and ^{15}N isotopic balances to evaluate the relative contribution of different sources of new nitrogen that support the observed particle export at stations SEATS and SS1, located respectively in the northern and southern basin of the SCS with different hydrological features. We showed that more than 50 % of the particle flux out of the NDL was supported by nitrate sources likely supplied from depth and associated with episodic intrusions other than atmospheric deposition and nitrogen fixation. However, the exact mechanisms and pathways for subsurface nutrients to support the export production from the NDL merit additional careful and dedicated studies.

1 Introduction

The marine biological carbon pump (BCP) plays a central role in sequestrating atmospheric CO_2, thereby mitigating human-induced climate change. Despite great efforts that have been devoted to studying the BCP, there remain critical knowledge gaps in terms of its structure, function and efficiency (Siegel et al., 2021). Recently, the EXPORTS (EXport Processes in the Ocean from RemoTe Sensing) program has implemented comprehensive experiments which examine export flux pathways, plankton community composition, food web processes and biogeochemical properties of the ecosys-

tem to achieve an improved understanding of export fluxes and the BCP (Siegel et al., 2016, 2021).

Among other factors, depth-dependent particle export at different horizons within the euphotic zone (Ez), and how these exports are sustained by different nutrient sources, remains largely unknown. Most previous studies have treated the Ez as a single box and chose a fixed depth (e.g., 100 or 150 m) as the export horizon (Benitez-Nelson et al., 2001; Cai et al., 2015; Zhou et al., 2020a). A recent study has suggested that using a fixed depth instead of the in situ Ez depth as the export horizon would lead to the magnitude of global POC export flux being underestimated by a factor of 2 (Buesseler et al., 2020a). In the oligotrophic oceans, permanent stratification limits nutrient supply from depth; the Ez thus could be divided into the following two-layer structure based on nutrient concentrations: (1) the nutrient-depleted layer (NDL) between the ocean surface and the top of the nutricline and (2) the nutrient-replete layer (NRL) between the nutricline and the base of the Ez (Du et al., 2017). Conventional concepts suggest that regenerated nutrients predominantly support biological productivity in the NDL, where export production is limited due to the absence of new nutrient supplies (Eppley and Peterson, 1979; Goldman, 1984). Meanwhile, Coale and Bruland (1987) noticed the layered structure of ^{234}Th–^{238}U disequilibria in the Ez, composed of an upper oligotrophic layer characterized by low new-production values and low net scavenging and a subsurface eutrophic layer with higher new-production values, and they suggested that new production rather than total primary production determined the scavenging of the reactive elements such as ^{234}Th. Cai et al. (2008) also observed variable particle-scavenging rates in the upper euphotic zone (above 50 m) but consistently lower rates in the lower euphotic zone (between 50 and 100 m) in the oligotrophic South China Sea (SCS). With increasing high-resolution samplings, such partitionings of ^{234}Th-based particle scavenging were frequently observable in oligotrophic ecosystems (Buesseler et al., 2009; Umhau et al., 2019; Zhou et al., 2020a; Stukel et al., 2022).

Along with the increasing attention on BCP in the oligotrophic ecosystems, some observations have, however, indicated that particles sourced from surface waters with extremely low nutrient concentrations may substantially contribute to the downward fluxes at depth. Scharek et al. (1999) observed that the diatom–diazotroph assemblages (*Hemiaulus hauckii* contained *Richelia*-type endosymbionts with heterocysts) in the surface nutrient-deficient mixed layer dominated downward particle fluxes collected by a sediment trap at 150 m depth at the oligotrophic station ALOHA (A Long-term Oligotrophic Habitat Assessment; 22°45′ N, 158° W). Liu et al. (2007) observed consistent $\delta^{13}C_{POC}$ values between sediment trap samples collected at 100 m and suspended particles in the upper 20 m in the SCS basin, likely suggesting that the trapped particles predominantly originated from the surface (i.e., 20 m). The ecosystem in

nutrient-depleted surface waters may therefore play an important role in carbon export. Different pathways to introduce new nutrients have been suggested to support the carbon export from the NDL; for example, high rates of nitrogen fixation in the NDL could support 26 %–47 % of the particle fluxes at station ALOHA (Böttjer et al., 2017). In addition, episodic eddy events that uplift the nutricline and deliver deep stocks of nutrients to the NDL might also contribute to POC export from the upper ocean (Johnson et al., 2010). Nevertheless, it remains unclear how the different nutrient supplies to the surface waters affect the downward POC export flux at the NDL and Ez horizons.

The semi-enclosed SCS, the largest marginal sea in the North Pacific Ocean, is characterized by an oligotrophic basin due to intensive stratification (Du et al., 2017). Several previous studies quantified the ^{234}Th-based POC export flux and explored the mechanisms controlling export in the SCS. Seasonally, POC export fluxes are elevated in winter, driven by the deepening of the mixed layer and nutrient supply from depth (Zhou et al., 2020a). Spatially, Cai et al. (2015) found that POC export fluxes decreased with distance offshore in the northern SCS due to reduced POC stocks. Mesoscale processes can also promote POC export by pumping nutrient-replete waters from depth into the Ez (Zhou et al., 2013, 2020b). Regardless, POC export fluxes at different export horizons, and the sources of new nutrients that support export, remain understudied in the oligotrophic SCS.

In this study, we conducted samplings of ^{234}Th at a reasonably high depth resolution in the Ez during the summer of 2017 to examine the structure of export productivity partitioning in the SCS basin. We calculated POC export fluxes based on ^{234}Th from both the NDL and Ez. Based on trap-derived masses and ^{15}N isotopic balances, we estimated the relative contributions of different nutrient sources to export fluxes within the two-layer nutrient-based structure in the SCS at two stations with different hydrological features. Moreover, we related POC export fluxes from the two layers to their different biogeochemical forcings (especially the depth of the nutricline and the subsurface nutrient concentrations) to examine the controlling factors that potentially regulate POC export flux in the oligotrophic SCS.

2 Methods

2.1 Sample collection

Ship-based sampling was conducted from 5 to 27 June 2017 on the R/V Tan *Kah Kee* in the SCS basin (Fig. 1 and Table 1) under the umbrella of the CHOICE-C II project (Carbon Cycle in the South China Sea: budget, controls and global implications). We visited two mega stations (SEATS and SS1) and nine regular stations during the cruise. The in situ observation at station SEATS was conducted before a typhoon (Merbok) which potentially affected the biogeochemistry of
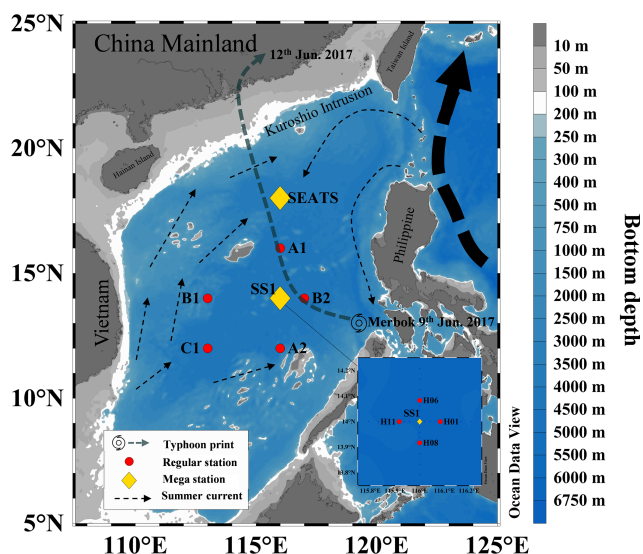
Figure 1. Map of the South China Sea (SCS) with sampling stations during June 2017. Yellow diamonds denote mega stations (SEATS and SS1) where high-resolution sampling was conducted at a 10 m interval in the euphotic zone; red circles denote regular stations where samples were collected at typical sampling depths of 5, 25, 50, 75 and 100 m. The general circulation pattern (adapted from Liu et al., 2016) is also shown. The dominant summer currents are denoted by dashed black arrows. The dashed dark-blue line denotes the path of the typhoon Merbok (generated at the southeastern part of the SCS on 9 June 2017).

the region, and the remaining stations were visited after the typhoon (listed in Table 1). To examine the spatial variability of ^{234}Th, we sampled four closely clustered stations (H01, H06, H08 and H11) around station SS1. Seawater samples were collected using 12 or 10 L Niskin bottles attached to a Sea-Bird 911 conductivity–temperature–depth (CTD) profiler.

At the mega stations, high-vertical-resolution water samples were taken at a depth interval of 10 m within the Ez. For regular stations, lower-resolution (5, 25, 50, 75 and 100 m) samples were collected. Seawater volumes of 4 and 8 L were collected for total ^{234}Th and particulate ^{234}Th/POC analysis, respectively. Samples were collected using acid-cleaned 4 L fluorinated bottles and filtered onto quartz microfiber (QMA) filters (25 mm diameter, 1.0 µm pore size). An amount of 500 mL of seawater was also collected for nutrient analysis from the Niskin bottles. Ancillary parameters, including potential temperature, salinity and fluorescence, were accessed using a Sea-Bird CTD sensor. We calibrated the sensor-derived fluorescence with the Chl a concentrations from discrete samples using the equation Chl a (mg m^{-3}) = 0.855 × fluorescence ($R^2 = 0.87$, $n = 139$; Fig. S1 in the Supplement).

In addition, we deployed an array of floating sediment traps for 72 h at 50, 100 and 200 m at both mega stations, SEATS and SS1, to collect sinking particles during the survey. Retrieval of the trap at station SS1 was precluded by unfavorable sea conditions. Consequently, we utilized sediment trap data acquired during a 53 h deployment in July 2019. Our choice of alternative data collection is unlikely to engender bias in our analysis, as evidenced by the limited inter-annual variability in ^{15}N signals of sinking particles obtained from sediment traps (see details in Sect. 3.5). At each depth of stations SEATS and SS1, 12 cylindrical acrylic tubes (with a height of 50 cm and diameter of 10 cm) were assembled for different biogeochemical measurements. Before deployment, the tubes were filled with prefiltered surface seawater, and NaCl was added to supersaturation. After recovery, the tubes were stored at temperatures under 4 °C until the particles settled to the bottom. After removing the overlying supernatant, the particles were prefiltered through Nitex filters (120 µm pore size) to remove the visible zooplankton and were then collected on QMA filters (1.0 µm pore size) for elemental and isotopic analyses.

2.2 ^{234}Th analysis

The small-volume (4 L) MnO$_2$ co-precipitation method was used for the total ^{234}Th analysis (Benitez-Nelson et al., 2001; Cai et al., 2006). The efficiency of thorium precipitation was monitored by ^{230}Th. In detail, the seawater samples were acidified after collection and spiked with 200 µL of ^{230}Th (17.38 dpm mL^{-1}). After an 8 h period to allow equilibration between samples and tracers, the pH of seawater was raised to 8.05–8.20 using NH$_3$·H$_2$O before 0.375 mL KMnO$_4$ (3.0 g L^{-1}) and 0.20 mL MnCl$_2$ (8.0 g L^{-1}) were added. The MnO$_2$ precipitates were collected for a total ^{234}Th analysis. The particles filtered for particulate ^{234}Th from the seawater samples on a QMA filter (25 mm, 1.0 µm) were dried in the oven overnight under 45 °C. The filters were then packed with Teflon rings and disks (diameter of 23.5 cm, produced by RISØ National Laboratory, Denmark) covered by aluminum foil (density: 6.45 mg m^{-2}) and Mylar film. A gas-flow-proportional low-level RISØ beta counter (model GM-25-5) was used for ^{234}Th counting. The first count was carried out immediately after the samples were set up, and the second count was carried out after > 6 months for the background measurement. All ^{234}Th samples were counted for 1000 min each time. The ^{230}Th recoveries were determined by inductively coupled plasma mass spectrometry (ICP-MS) (Agilent 7700x). The average of all the recoveries was 88 ± 12 % (mean ± 1σ, $n = 97$, range 73 %–98 %). All ^{234}Th data were recovery- and decay-corrected to the sampling time. The uncertainties of ^{234}Th data were propagated from the counting error, uncertainty from recovery and detection efficiency. The ^{238}U activity was estimated by the following equation assuming conservative behavior with respect to salinity (Owens et al., 2011):

$$^{238}\text{U} = 0.0786 \times S - 0.314. \tag{1}$$

Table 1. Sampling logs and site information along with the accessed parameters and their utilizations.

Station	Arriving time [UTC+8]	Latitude [° N]	Longitude [° E]	Bottom depth [m]	Total ^{234}Th	Trap	Partitioning POC flux estimate	Nutrient source diagnosis
					Parameters		Data utilizations	
SEATS	7 Jun 2017, 00:06	18.0	116.0	3907	√	√	√	√
A1*	11 Jun 2017, 23:55	16.0	116.0	4205	√		√	
SS1	12 Jun 2017, 20:08	14.0	116.0	4107	√		√	
H06	20 Jun 2017, 02:28	14.1	116.0	4289	√		√	
H08	20 Jun 2017, 07:51	13.9	116.0	4063	√		√	
H01	20 Jun 2017, 23:41	14.0	116.1	4139	√		√	
H11	21 Jun 2017, 05:18	14.0	115.9	4297	√		√	
B1	22 Jun 2017, 11:43	14.0	113.0	2537	√		√	
C1	23 Jun 2017, 04:40	12.0	113.0	4313	√		√	
A2	24 Jun 2017, 03:05	12.0	116.0	4079	√		√	
B2	24 Jun 2017, 21:42	14.0	117.0	3947	√		√	

* Sampling station might be influenced by the typhoon event passing through the South China Sea. Station A1 was visited right after the typhoon Merbok, which was generated on 9 June 2017 at 13.1° N, 119.8° E in the southern South China Sea. Merbok landed on 12 June at 27.5° N, 117.3° E.

2.3 POC, PN and $\delta^{15}N_{PN}$ analyses

Upon ^{234}Th counting, the particulate samples were carefully removed from the disks and placed in glass dishes. Subsequently, the filters were dried at 50 °C for 24 h after adding 0.4 mL of HCl (1.0 µmol L^{-1}) to remove inorganic carbon. POC and particulate nitrogen (PN) concentrations were determined by an elemental analyzer-isotope ratio mass spectrometer (EA-IRMS) system (EA: vario PYRO cube; IRMS: Isoprime 100). At station SS1, we conducted 10 replicate POC samplings at 5, 100 and 200 m water depth to investigate the precision of bottle-collected POC. Our results show that the standard deviations of our analyses were better than 13 %, which agrees well with the result from the JGOFS cookbook (Knap et al., 1996). The errors were included in the subsequent calculation of POC export fluxes. The particles from the sediment traps were treated the same as the suspended particles. The C and N contents and the isotopes of sinking particles were also analyzed by EA-IRMS.

2.4 The depth of the euphotic zone

The euphotic zone depth (Zeu or the Ez base, in m) is defined optically, based on Wu et al. (2021), as the depth where the usable solar radiation (USR) equals 0.9 % of the surface USR, which is close to the depth where the photosynthetically available radiation (PAR) equals 0.5 % of the PAR value at the sea surface. In situ Zeu during the cruise was obtained from profiling PAR data recorded by the optical sensor (Biospherical QCP2300-HP) on the CTD.

2.5 Nutrient analysis and nutricline depth

Nutrients were analyzed on board using a Four-channel Continuous Flow Technicon AA3 Auto-Analyzer (Bran-Lube

GmbH). The detection limits for both N + N (nitrate plus nitrite – termed as dissolved inorganic nitrogen, DIN) and dissolved inorganic phosphorus (DIP) were 0.03 µmol L^{-1}. The top of the nutricline in this study was defined as the depth at which the DIN concentration reached 0.1 µmol L^{-1} (Dore and Karl, 1996; Winn et al., 1995). The layers above and below to the base of Ez were defined as the as NDL and NRL, respectively.

2.6 ^{234}Th scavenging model

The mass balance for ^{234}Th in seawater can be described using Eq. (1) (Buesseler et al., 1992):

$$\frac{\partial A_{Th}^{total}}{\partial t} = \lambda \left(A_U - A_{Th}^{total} \right) - F_{Th} + V,$$ (2)

where F_{Th} is the ^{234}Th scavenging flux at the export horizon. A_U and A_{Th}^{total} are the ^{238}U and total ^{234}Th activities, and λ is the ^{234}Th decay constant (0.02876 d^{-1}); V, which is discussed below, is the term for physical effects, including advection and diffusion.

For particle export from the Ez, the deficit of total ^{234}Th relative to ^{238}U is integrated with depth to evaluate ^{234}Th fluxes. Under the assumption of a steady state ($\frac{\partial A_{Th}^{total}}{\partial t} = 0$) and no physical transport ($V = 0$), the ^{234}Th export flux from the Ez (F_{Th}^{Ez}) is integrated by Eq. (3) (as shown in Fig. 2):

$$F_{Th}^{Ez} = \int_0^{Ez} (A_U - A_{Th}) \times \lambda dz.$$ (3)
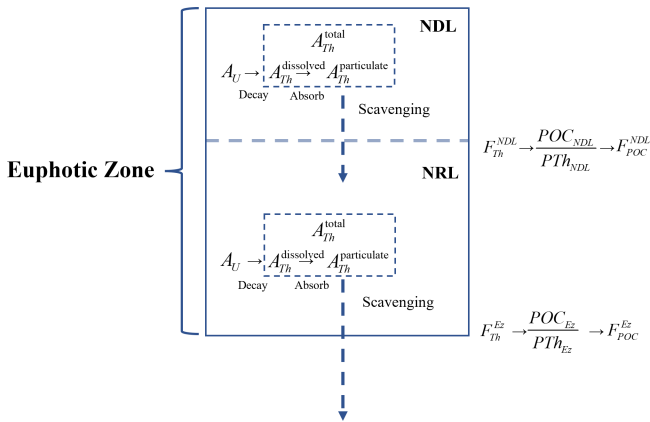
Figure 2. Schematic of the ^{234}Th model under the two-layer nutrient structure. The terms are defined in Eqs. (2)–(4) and (7)–(9).

Similarly, ^{234}Th export flux from the base of the NDL, $F_{\mathrm{Th}}^{\mathrm{NDL}}$, is estimated as follows:

$$F_{\mathrm{Th}}^{\mathrm{NDL}} = \int_{0}^{\mathrm{NDL}} (A_{\mathrm{U}} - A_{\mathrm{Th}}) \times \lambda \mathrm{d}z. \tag{4}$$

However, the assumption of no physical transport needs to be verified before ^{234}Th flux is calculated. In this study, the physical transport is estimated as follows:

$$V = -u \times \frac{\partial A_{\mathrm{Th}}}{\partial x} - v \times \frac{\partial A_{\mathrm{Th}}}{\partial y} - w \times \frac{\partial A_{\mathrm{Th}}}{\partial z}$$
$$+ K_x \frac{\partial^2 A_{\mathrm{Th}}}{\partial x^2} + K_y \frac{\partial^2 A_{\mathrm{Th}}}{\partial y^2} + K_z \frac{\partial^2 A_{\mathrm{Th}}}{\partial z^2}, \tag{5}$$

where u, v and w are the zonal, meridional and upwelling velocities, respectively; $\frac{\partial A_{\mathrm{Th}}}{\partial x}$, $\frac{\partial A_{\mathrm{Th}}}{\partial y}$ and $\frac{\partial A_{\mathrm{Th}}}{\partial z}$ are ^{234}Th activity gradients from west to east, south to north and upward. K_x, K_y and K_z are diffusivities from west to east, south to north and upward, respectively, and $\frac{\partial^2 A_{\mathrm{Th}}}{\partial x^2}$ and $\frac{\partial^2 A_{\mathrm{Th}}}{\partial z^2}$ are the second derivatives of ^{234}Th activity distributions (Benitez-Nelson et al., 2001; Cai et al., 2008; Buesseler et al., 2020b).

To better constrain the ^{234}Th flux in the SCS basin, we estimated the horizontal and vertical transports of ^{234}Th at the station SS1. The climatological w and K_z from modeling results (Gan et al., 2016) were applied to the equation to evaluate the impacts of vertical advection and diffusion on the ^{234}Th flux. The vertical transport fluxes were -2.0 ± 0.4 and $-11.4 \pm 0.1 \, \mathrm{dpm \, m^{-2} \, d^{-1}}$ at the bases of the NDL and Ez, respectively, which can be considered to be negligible (less than 10 %) compared to the vertical scavenging flux at the station SS1. This was in agreement with Cai et al. (2008), who also showed that the vertical term could be neglected for ^{234}Th flux estimation in the SCS basin.

The apparent diffusivity around station SS1 is estimated as $\sim 4 \times 10^5 \, \mathrm{cm^2 \, s^{-1}}$ (Okubo, 1971) from empirically derived oceanic-diffusion diagrams, and we simplified the horizontal diffusive term in Eq. (5) based on Benitez-Nelson et al. (2000) as follows:

$$V_{\mathrm{diffusion}} = \left[\frac{[K_x (A_{\mathrm{Th\text{-}H11}} - 2 \times A_{\mathrm{Th\text{-}SS1}} + A_{\mathrm{Th\text{-}H01}})]^2}{\Delta x^2} \right.$$
$$\left. + \frac{[K_y (A_{\mathrm{Th\text{-}H08}} - 2 \times A_{\mathrm{Th\text{-}SS1}} + A_{\mathrm{Th\text{-}H06}})]^2}{\Delta y^2} \right]^{1/2}. \tag{6}$$

The Δx and Δy are the distance between the stations to evaluate the influences of physical terms (i.e., Δx is the distance between stations H01 and H11; Δy is the distance between stations H06 and H08). Δx and Δy were equal to 18 km in this study. Thus, the ^{234}Th flux derived from horizontal diffusion was considerably low (approximately $0.1 \, \mathrm{dpm \, m^{-2} \, d^{-1}}$).

The in situ horizontal current velocities at station SS1 from the acoustic Doppler current profiler (ADCP) exhibited a wide range from 0.01 to 0.3 $\mathrm{m \, s^{-1}}$ in the upper 200 m. Since these current velocities were measured instantaneously and since their timescales did not match those of ^{234}Th (~ 20 d), we applied model-derived time-integrated data (3-month average) to the equation instead. The model-derived u and v ranged from 0.007 to 0.2 $\mathrm{m \, s^{-1}}$ in the upper 100 m. Based on those velocities, the ^{234}Th flux from horizontal transport was about 15 % of the ^{234}Th flux estimated using the steady-state model in the upper 100 m, which is consistent with previous studies in oligotrophic ecosystems (e.g., Cai et al., 2008; Buesseler et al., 2020b). Thus, a 1D model assumption is applicable in this study for the subsequent ^{234}Th flux estimation.

2.7 POC export flux calculation

In this study, the ^{234}Th-derived POC export flux was calculated using the following equations:

$$F_{\mathrm{POC}}^{\mathrm{Ez}} = F_{\mathrm{Th}}^{\mathrm{Ez}} \times \frac{\mathrm{POC_{Ez}}}{\mathrm{PTh_{Ez}}}, \tag{7}$$

where $F_{\mathrm{Th}}^{\mathrm{Ez}}$, $\frac{\mathrm{POC_{Ez}}}{\mathrm{PTh_{Ez}}}$ and $F_{\mathrm{POC}}^{\mathrm{Ez}}$ are the ^{234}Th flux, particulate POC/^{234}Th ratio and POC flux at the Ez base, respectively;

$$F_{\mathrm{POC}}^{\mathrm{NDL}} = F_{\mathrm{Th}}^{\mathrm{NDL}} \times \frac{\mathrm{POC_{NDL}}}{\mathrm{PTh_{NDL}}}, \tag{8}$$

where $F_{\mathrm{Th}}^{\mathrm{NDL}}$, $\frac{\mathrm{POC_{NDL}}}{\mathrm{PTh_{NDL}}}$ and $F_{\mathrm{POC}}^{\mathrm{NDL}}$ are the ^{234}Th flux, particulate POC/^{234}Th ratio and POC export flux at the NDL base, respectively.

Sediment-trap-derived POC export fluxes were calculated as follows:

$$F_{\mathrm{POC\text{-}Trap}} = \frac{\mathrm{POC_{Measured}}}{\Delta t \times A_{\mathrm{TrapTube}}}, \tag{9}$$

where POC is the concentration of organic carbon on the particles collected by the traps, Δt is the duration of trap deployments, and A_{TrapTube} is the area of the trap tube.

3 Results

3.1 Environmental settings

The profiles of temperature and salinity reveal distinctive hydrological features between stations in the SCS basin (Fig. 3). The surface mixed-layer depth (MLD, defined as the depth where the potential density σ_θ increased by $0.03\,\mathrm{kg\,m^{-3}}$ compared to the value at the sea surface; Cornec et al., 2021) at stations SEATS, A1, A2 and C1 was shallower (20–39 m) than at other stations (MDL > 40 m; Table 2 and Fig. 3). The shallower MLD and isoclines (i.e., thermocline and halocline) might indicate upward displacement of waters at those stations. Du et al. (2021) attributed such vertical shifts in isoclines to mesoscale processes or basin-scale circulation. Indeed, most of these stations (SEATS, A1 and C1) were under the influence of eddies during the sampling periods, as revealed by the sea level anomaly (SLA) map (Fig. S2 in the Supplement); modeling results indicate stations C1 and A2 were impacted by cold water sourced from the southwestern SCS basin and derived from upwelling off the coast of Vietnam (Fig. S3 in the Supplement) (Gan et al., 2016).

As shown in Fig. 3c, nutrients were depleted in surface waters until the top of the nutriclines, where concentrations started to rapidly increase. The depth profiles also show a clear relationship between nutriclines and subsurface nutrient concentrations. The four stations (i.e., stations SEATS, C1, A1 and A2) with shallower nutriclines correspond well with higher subsurface nutrient concentrations. For example, DIN concentrations at 125 m in these four sites ranged from 13.1 to $17.0\,\mathrm{\mu mol\,N\,L^{-1}}$, averaged at $14.0\pm2.1\,\mathrm{\mu mol\,N\,L^{-1}}$; in contrast, DIN concentrations at the same depth in other sites with deeper nutriclines ranged from 6.5 to $12.1\,\mathrm{\mu mol\,N\,L^{-1}}$, averaged at $8.9\pm2.4\,\mathrm{\mu mol\,N\,L^{-1}}$ (Fig. 3c).

The partitioned nutrient inventories (i.e., nutrient inventories within the NDL and Ez) also showed such a trend (Fig. 4a, b). The average Ez inventory of DIN was $196\pm30\,\mathrm{mmol\,N\,m^{-2}}$ at stations with shallow nutriclines compared to $29\pm19\,\mathrm{mmol\,N\,m^{-2}}$ at other stations, and the average inventory of PO_4^{3-} (DIP) in the Ez at stations with shallow nutriclines was $13\pm1\,\mathrm{mmol\,P\,m^{-2}}$ compared to an average of $3\pm2\,\mathrm{mmol\,P\,m^{-2}}$ at other stations. The pattern of nutrient inventories across stations possibly results from vertical water displacement induced by horizontal divergence at the mesoscale and/or basin scale (Du et al., 2021).

Chl a concentrations at the four stations with shallower nutriclines were consistently enhanced in response to elevated nutrient levels, resulting in shallower depths of subsurface Chl a maxima (SCM; Fig. 3d) relative to other stations (55–80 m vs. 85–108 m). Chl a inventories at these stations with high nutrient inventories (23.6–52.2 mg m^{-2}, average $29.6\pm4.8\,\mathrm{mg\,m^{-2}}$) were significantly higher ($p < 0.05$) than at others stations (8.0–22.8 mg m^{-2}, average $14.0\pm4.6\,\mathrm{mg\,m^{-2}}$; Fig. 4c).

3.2 ^{234}Th and POC variability

Variations of total ^{234}Th and Chl a versus depth are shown in Fig. 5. The activities of total ^{234}Th ranged from 1.70 ± 0.05 to $2.73\pm0.05\,\mathrm{dpm\,L^{-1}}$, with an average of $2.30\pm0.31\,\mathrm{dpm\,L^{-1}}$ ($n = 97$; Fig. 5), and all stations displayed similar patterns. Generally, ^{234}Th was deficient relative to ^{238}U in the upper Ez and was in equilibrium or excess at the base of and/or below the Ez. The ^{234}Th deficit peaked within the NDL and largely diminished in the NRL, implying that a large amount of particle removal occurred in the NDL but that low export or high remineralization occurred in the NRL. The ^{234}Th activity minimum ($1.70\pm0.17\,\mathrm{dpm\,L^{-1}}$) appeared at a depth of 25 m at station A1 (one of stations characterized by a shallow MLD and nutricline). ^{234}Th activity at the stations surrounding station SS1 showed little spatial variability: the differences in ^{234}Th activity were less than 0.1 dpm L^{-1} at the same depth.

Particulate ^{234}Th ranged from $0.13\pm0.01\,\mathrm{dpm\,L^{-1}}$ to $0.47\pm0.01\,\mathrm{dpm\,L^{-1}}$ (with an average of $0.25\pm0.11\,\mathrm{dpm\,L^{-1}}$, $n = 83$; Fig. 6). At most stations, the profiles of particulate ^{234}Th shared similar depth patterns with Chl a, with the maximum values appearing in the subsurface water, while at stations H01 and H06, particulate ^{234}Th generally increased with depth in the upper 100 m and showed little station-to-station variability. The maximum of particulate ^{234}Th appearing at both the surface and subsurface at station B2 suggested complicated biogeochemistry of ^{234}Th on particles.

POC concentrations ranged from 0.83 to $2.5\,\mathrm{\mu mol\,L^{-1}}$ (with an average of $1.2\pm0.44\,\mathrm{\mu mol\,L^{-1}}$, $n = 83$; Fig. 6). At most stations, the POC concentration was low (with an average of $1.1\pm0.2\,\mathrm{\mu mol\,L^{-1}}$) in surface water and generally increased with depth until it reached its maximum at the SCM layer, and then it decreased again with depth. However, at some stations (i.e., C1, B2), there were POC peaks that appeared in both the surface water and the SCM layer.

3.3 Water-column-integrated and sediment-trap-derived ^{234}Th fluxes

Calculated ^{234}Th fluxes at different export horizons (i.e., the NDL and Ez base) are shown in both Table 2 and Fig. 4d. ^{234}Th fluxes at the Ez base mostly ranged from 267 ± 69 to $839\pm59\,\mathrm{dpm\,m^{-2}\,d^{-1}}$. ^{234}Th fluxes at the NDL base ranged from 204 ± 57 to $624\pm52\,\mathrm{dpm\,m^{-2}\,d^{-1}}$, which accounts for 69 %–100 % of ^{234}Th fluxes at the Ez base. We found that the ^{234}Th fluxes remained rather low, mostly $< 800\,\mathrm{dpm\,m^{-2}\,d^{-1}}$, during our study, which was close to the threshold for the validity of the steady-state assumption, as shown in many prior studies (e.g., Savoye et al., 2006; Resplandy et al., 2012). The sea surface Chl a also indicated that no bloom was observed during the survey in June 2017 (Fig. S4 in the Supplement), suggesting that the study area retained its biogeochemistry under the steady-state condition.
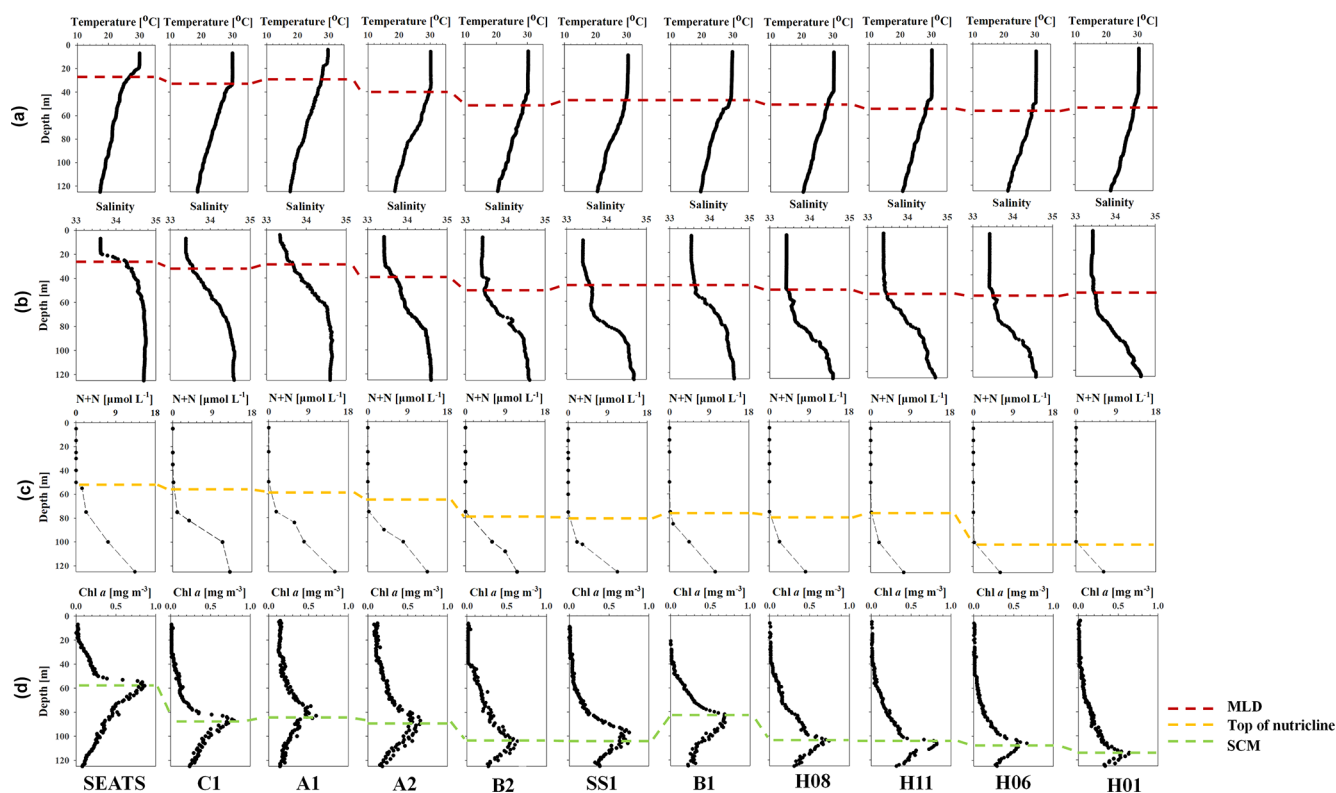
Figure 3. Vertical profiles of temperature (**a**), salinity (**b**), dissolved inorganic nitrogen (nitrate + nitrite; DIN) (**c**) and Chl a (**d**). The MLD (red dash), interpolated depth of DIN = $0.1\,\mu mol\,L^{-1}$ (top of nutricline, yellow dash) and subsurface Chl a maximum (SCM, green dash) are also shown.

Table 2. Surface mixed-layer depths (MLDs), export horizon depths, 1D steady-state ^{234}Th fluxes, POC/^{234}Th ratios and POC fluxes at stations in the upper oligotrophic South China Sea basin during June 2017.

Station	[a]MLD [m]	[b]NDL base [m]	[c]Ez base [m]	^{234}Th flux @ NDL dpm m^{-2} d^{-1}	^{234}Th flux @ Ez dpm m^{-2} d^{-1}	POC/^{234}Th ratio @ NDL μmol C dpm^{-1}	POC/^{234}Th @ Ez μmol C dpm^{-1}	POC export flux @ NDL mmol C m^{-2} d^{-1}	POC export flux @ Ez mmol C m^{-2} d^{-1}
SEATS	27	50	80	362 ± 34	522 ± 43	4.4 ± 0.6	5.5 ± 0.7	1.6 ± 0.6	2.9 ± 0.7
C1	36	59	87	598 ± 57	602 ± 22	6.2 ± 0.8	2.9 ± 0.4	3.7 ± 0.9	1.7 ± 0.4
A1	27	57	88	603 ± 98	585 ± 100	7.1 ± 0.9	5.2 ± 0.7	4.3 ± 1.2	3.0 ± 0.8
A2	39	63	96	624 ± 52	839 ± 59	6.3 ± 0.8	2.7 ± 0.3	3.9 ± 0.9	2.2 ± 0.4
B2	44	71	102	204 ± 57	267 ± 69	8.2 ± 1.1	8.3 ± 1.1	1.7 ± 1.2	2.2 ± 1.2
SS1	43	81	111	613 ± 42	631 ± 48	4.0 ± 0.5	3.1 ± 0.4	2.4 ± 0.5	2.0 ± 0.4
B1	50	78	87	361 ± 63	421 ± 64	4.1 ± 0.5	3.8 ± 0.5	1.5 ± 0.6	1.6 ± 0.6
H08	42	80	106	376 ± 61	462 ± 68	5.8 ± 0.8	4.6 ± 0.6	2.2 ± 0.8	2.1 ± 0.7
H11	48	82	106	360 ± 61	393 ± 66	3.2 ± 0.4	4.1 ± 0.5	1.1 ± 0.5	1.6 ± 0.6
H06	52	87	115	439 ± 63	462 ± 66	3.2 ± 0.4	2.8 ± 0.4	1.4 ± 0.5	1.3 ± 0.4
H01	48	99	107	351 ± 70	350 ± 70	3.3 ± 0.4	3.3 ± 0.4	1.2 ± 0.5	1.2 ± 0.5

[a] The MLD is defined as the depth where the potential density σ_θ increases by $0.03\,kg\,m^{-3}$ compared to values at the sea surface (Cornec et al., 2021). [b] The NDL base, or the top of the nutricline, was interpolated to the depth where DIN = $0.1\,\mu mol\,L^{-1}$ based on the DIN distribution near the SCM. [c] The Ez base is estimated to be the depth where PAR is 0.5 % of the PAR value at the sea surface.

^{234}Th fluxes at the Ez base were within the range of 62–1365 dpm m^{-2} d^{-1}, similar to those found in prior studies in the SCS basin (e.g., Cai et al., 2008, 2015; Zhou et al., 2013, 2020a). Given that our high-vertical-resolution sampling mode was only applied to stations SEATS and SS1, we

estimated ^{234}Th fluxes at the Ez base by reducing the vertical resolution to a 25 m interval so as to be consistent with other stations. This exercise resulted in values of 490 ± 60 and 655 ± 71 dpm m^{-2} d^{-1}, respectively, for stations SEATS and SS1 compared to 522 ± 43 and 631 ± 48 dpm m^{-2} d^{-1} under
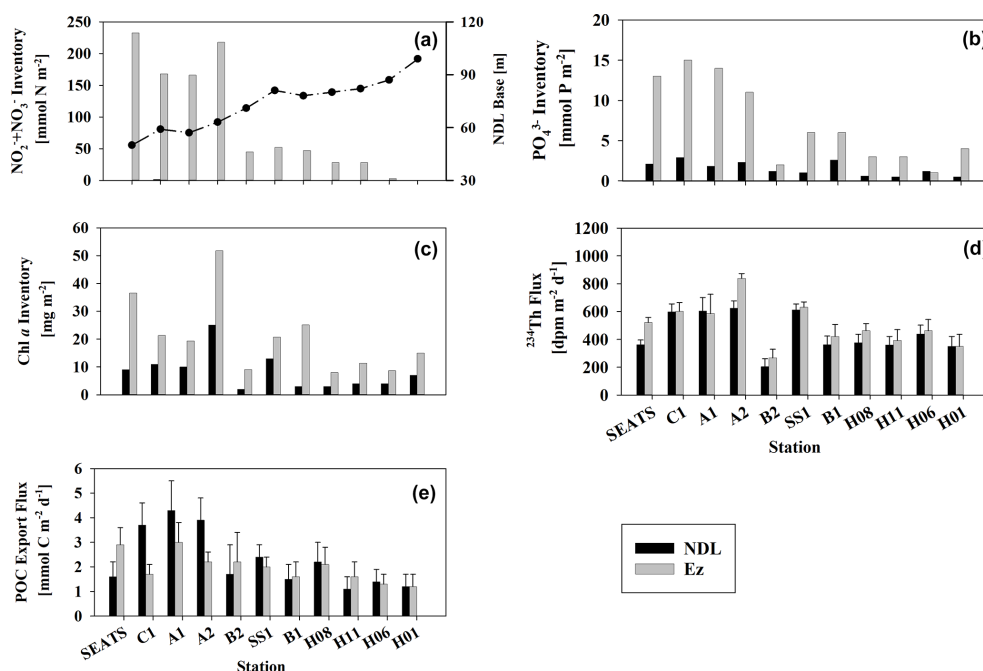
Figure 4. Integrated inventories of DIN (**a**) and DIP (**b**) in both the NDL (black) and Ez (gray). Also shown are the partitioned Chl a stocks (**c**), integrated partitioned ^{234}Th fluxes (**d**) and ^{234}Th-derived POC export fluxes (**e**). The high and low nutrient inventories correspond to shallow and deep nutriclines (**a**) (dotted line, NDL base), respectively.

the high-resolution sampling mode. The low-resolution sampling thus might induce an uncertainty of less than 6 % for the ^{234}Th flux. However, high-resolution sampling is essential in order to examine the partitioning of carbon export in the upper water column, especially for the oligotrophic ocean characteristic of low export fluxes.

Based on the high-resolution total ^{234}Th pattern at stations SEATS and SS1, we first determined the ^{234}Th deficit in the NDL, showing substantial particle scavenging and POC export at the NDL base at both stations, and we subsequently found similar patterns at the rest of stations where we estimated the partitioning in POC export fluxes.

Besides the ^{234}Th–^{238}U disequilibrium method, sediment-trap-derived ^{234}Th fluxes at SEATS were 589 ± 2 dpm m^{-2} d^{-1} at the NDL base (50 m), representing over 50 % of the ^{234}Th flux, and 830 ± 2 dpm m^{-2} d^{-1} near the Ez base (100 m). The trap-derived ^{234}Th fluxes were higher, but within a factor of 2, than the fluxes derived from bottle-sampled ^{234}Th (362 ± 34 dpm m^{-2} d^{-1} at 50 m and 471 ± 46 dpm m^{-2} d^{-1} at 100 m) at both export horizons. Although ^{234}Th fluxes at the base of the NDL had rarely been quantified in prior studies, we estimated the particle-scavenging rate at the corresponding export horizon with the historical data of ^{234}Th. Our recalculation using these literature data showed that ^{234}Th fluxes at the NDL base averaged 349 ± 296 dpm m^{-2} d^{-1} ($n = 36$) with limited spatial and temporal variations in the oligotrophic SCS. This is also consistent with the fact that these prior measurements

of ^{234}Th shared similarities in terms of activities in the NDL (Cai et al., 2015; Zhou et al., 2020a). Nevertheless, the partitioning in particle fluxes between the NDL and Ez, based on both techniques employed in this study, is similar, which further supports that our ^{234}Th–^{238}U-disequilibrium-based fluxes are representative.

3.4 POC/^{234}Th ratios based on bottle filtration and sediment traps

Bottle-derived POC/^{234}Th profiles in the Ez are shown in Fig. 7. They ranged from 2.6 to 15.7 µmol dpm^{-1} (with an average of 5.6 ± 3.3 µmol dpm^{-1}, $N = 83$), peaked in the upper 25 m and generally decreased with depth at all stations. POC/^{234}Th differences between most stations gradually diminished with depth and converged near 4.2 ± 1.6 µmol dpm^{-1} at the base of the Ez. The decreasing pattern of POC/^{234}Th was not observed at stations SEATS and H11 (as noted in Fig. 7a).

POC/^{234}Th ratios from sediment traps were only measured at station SEATS and were 4.7 and 3.2 µmol dpm^{-1} at 50 and 100 m, respectively (Fig. 7b). These values are comparable with the bottle-derived POC/^{234}Th ratios from the same site as that sampled during the cruise.

3.5 δ^{15}N$_{PN}$ from sediment traps

The δ^{15}N$_{PN}$ values for the trap samples varied between 2.6 ‰ to 6.7 ‰ in the upper 200 m at stations SEATS and
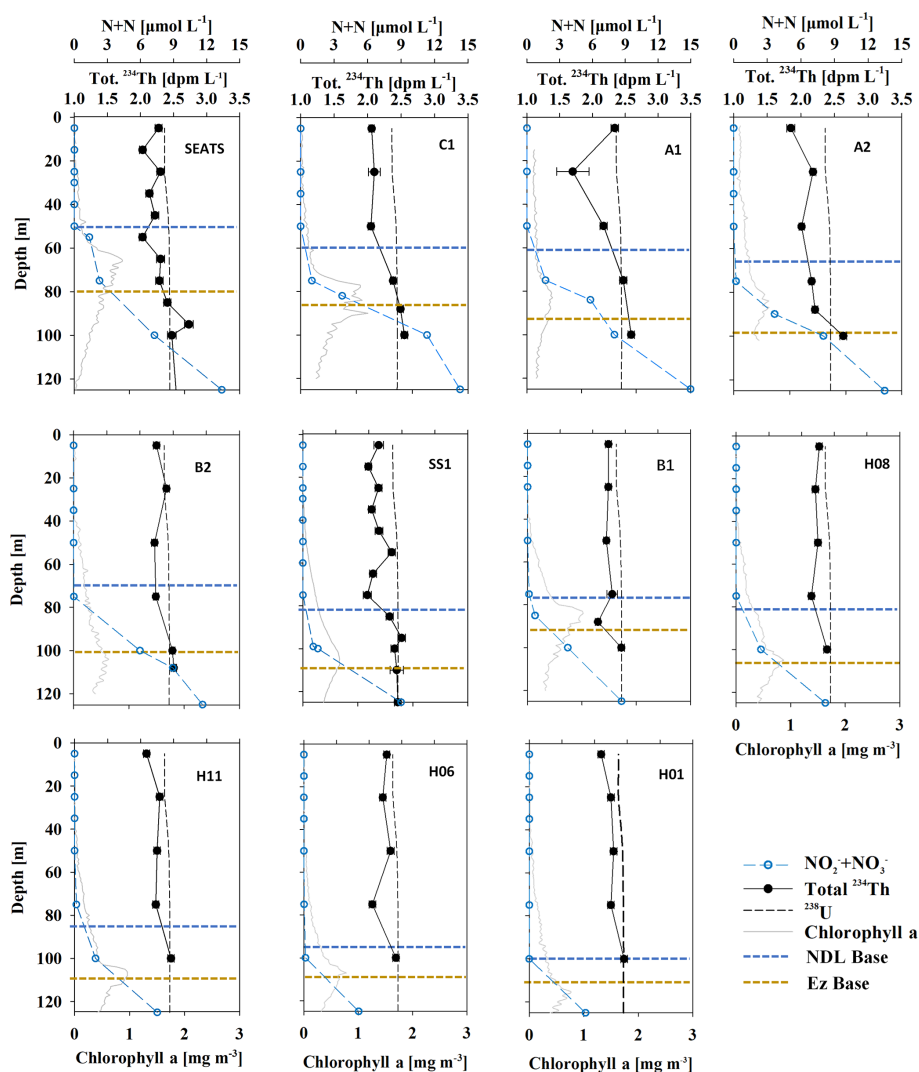
Figure 5. Depth profiles of DIN (open blue circle – $\mu mol\,L^{-1}$), total ^{234}Th activity (black dot – $dpm\,L^{-1}$), ^{238}U activity (black dash – $dpm\,L^{-1}$) and Chl a concentration (gray line – $mg\,m^{-3}$) in the South China Sea basin. The defined export horizons of the NDL base (blue dash) and the Ez base (yellow dash) are also shown. The deficit of ^{234}Th relative to ^{238}U was the most pronounced in the province where DIN was too low to be detected.

SS1, showing an increasing trend with depth. Specifically, the lowest $\delta^{15}N_{PN}$ of 2.6‰ was observed at 50 m within the NDL, and the $\delta^{15}N_{PN}$ increased to 4.7‰ at the Ez base (about 100 m). Below the Ez, the $\delta^{15}N_{PN}$ value increased to 6.7‰ at 200 m at station SEATS. A similar pattern of $\delta^{15}N_{PN}$ was also found at station SS1, with the lowest $\delta^{15}N_{PN}$ of 4.1‰ at 50 m, an intermediate value of 5.8‰ at 100 m and the highest value of 6.0‰ at 200 m. The observed $\delta^{15}N_{PN}$ values at both stations were comparable to previous results (3.3‰–7.3‰) from sinking particles collected by sediment traps in the upper 500 m around station SEATS (Kao et al., 2012; Yang et al., 2017). Yang et al. (2017) found a $\delta^{15}N_{PN}$ value of 4.9‰ at 100 m at station SEATS, which was very consistent with our observation at the same depth at station SEATS. These results suggest that interannual varia-

tions in $\delta^{15}N_{PN}$ from the upper ocean in the SCS may be limited, and the $\delta^{15}N_{PN}$ value at station SS1 from the cruise in 2019 could be comparable to that in this campaign. We thus diagnose the nutrient sources of sinking particles at stations with different environmental settings without focusing on temporal variability.

4 Discussion

4.1 ^{234}Th fluxes at the NDL and Ez bases

The particle flux at the NDL base was comparable ($88 \pm 11\%$) to that at the Ez base. This vertical structure indicates that the NDL base should be a hotspot for particle scavenging. The trap-derived ^{234}Th fluxes
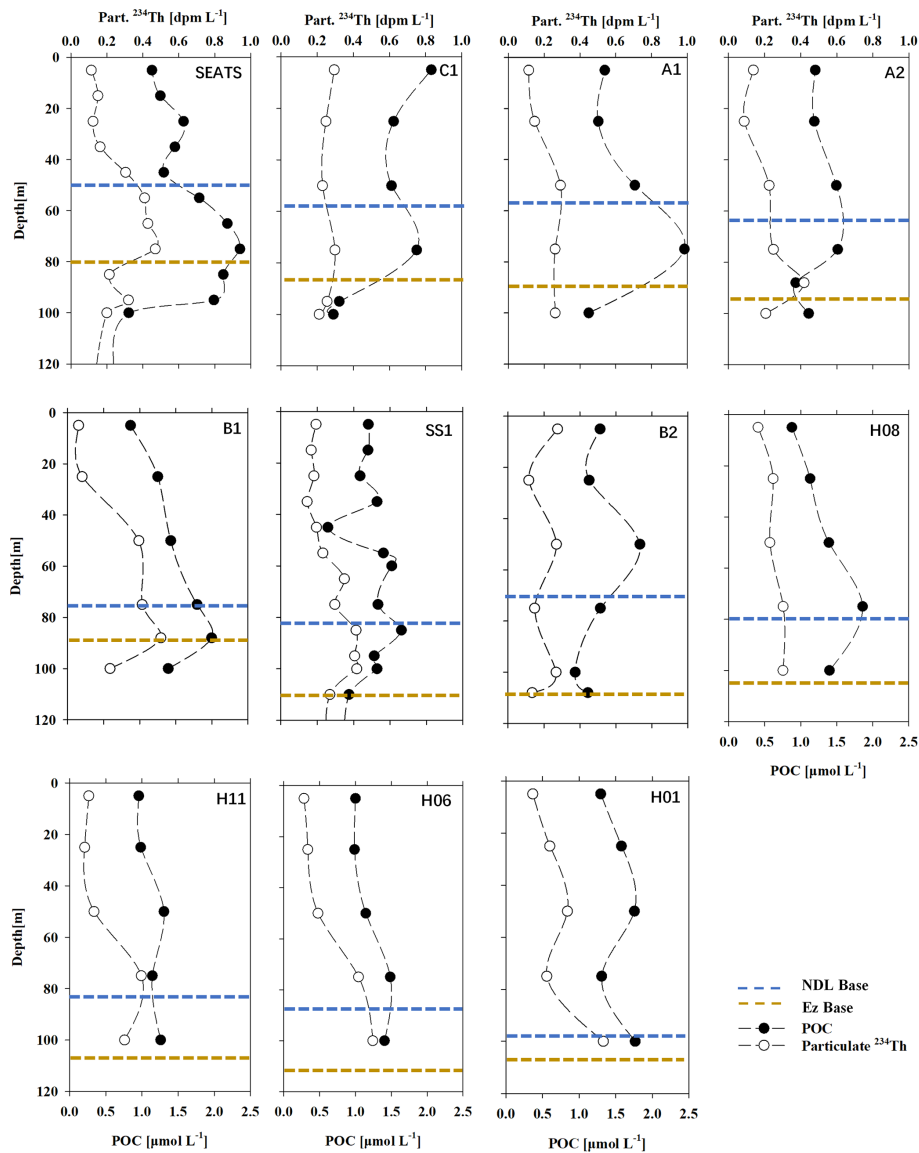
Figure 6. Profiles of POC (black dots – $\mu mol\,L^{-1}$) and particulate ^{234}Th activity (PTh, open circles – $dpm\,L^{-1}$) at all stations sampled in the South China Sea basin in June 2017. The bases of both the NDL (dashed blue line) and the Ez (dashed yellow line) are also shown.

($589 \pm 2\,dpm\,m^{-2}\,d^{-1}$ at 50 m and $830 \pm 2\,dpm\,m^{-2}\,d^{-1}$ at 100 m) were slightly higher compared to bottle-derived ^{234}Th fluxes ($362 \pm 34\,dpm\,m^{-2}\,d^{-1}$ at 50 m and $471 \pm 46\,dpm\,m^{-2}\,d^{-1}$ at 100 m). The higher trap-derived ^{234}Th fluxes might possibly be related to incomplete removal of zooplankton (Buesseler et al., 2020b). In addition, the discrepancy in between could be due to the difference in their timescales (Umhau et al., 2019). Regardless of the differences in ^{234}Th flux estimations from the separate methods, the similar vertical partitioning from both bottle- and trap-derived ^{234}Th fluxes indicated substantial particle scavenging at the bases of both the NDL and Ez in the oligotrophic SCS.

It is also interesting to note that, at stations with higher nutrient inventories, ^{234}Th fluxes (362 ± 34–$624 \pm 52\,dpm\,m^{-2}\,d^{-1}$, average $547 \pm 107\,dpm\,m^{-2}\,d^{-1}$ at the NDL base, and 522 ± 45–$839 \pm 59\,dpm\,m^{-2}\,d^{-1}$, average $637 \pm 120\,dpm\,m^{-2}\,d^{-1}$ at the Ez base) are significantly higher (by approximately 100–200 $dpm\,m^{-2}\,d^{-1}$) than those at other stations (210 ± 38–$520 \pm 31\,dpm\,m^{-2}\,d^{-1}$, average $359 \pm 90\,dpm\,m^{-2}\,d^{-1}$ at the NDL base, and 204 ± 57–$613 \pm 42\,dpm\,m^{-2}\,d^{-1}$, average $427 \pm 105\,dpm\,m^{-2}\,d^{-1}$ at the Ez base; Fig. 4d). This regional pattern of ^{234}Th fluxes might result from differences in nutrient distributions, as ^{234}Th has thus far been an indispensable tool to trace biogenic particle scavenging (Ceballos-Romero et al., 2022, and references therein). Whether these high and low ^{234}Th
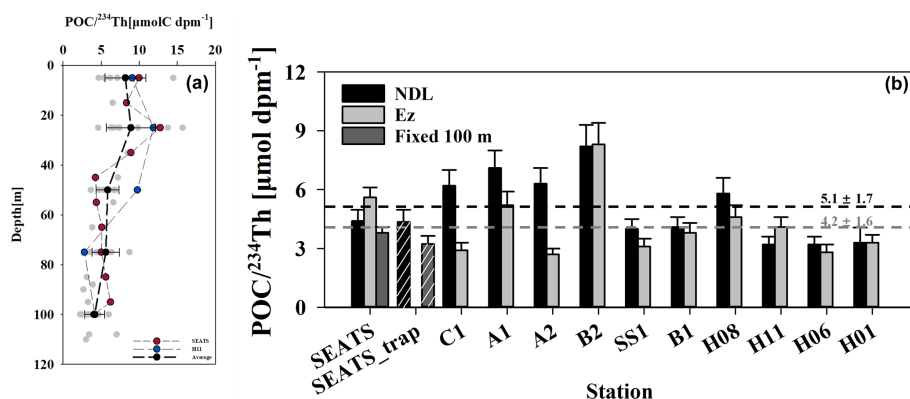
Figure 7. Water column POC/^{234}Th ratios from bottle filtration, with the averages (black dots with dashed line) at each sampling depth plotted against depth **(a)**. Also shown are the bottle- and trap-derived POC/^{234}Th ratios (bar with white stripes) at the bottom of the NDL (black), the base of the euphotic zone (light gray) and fixed 100 m depth (dark gray) **(b)**. Generally, the variability of POC/^{234}Th decreased as depth increased and converged around 4.2 ± 1.6 µmol dpm^{-1} at the Ez base. No significant variability (within a factor of 2) was found between POC/^{234}Th ratios derived from bottle and trap samples accessed at the same sampling depths at station SEATS.

fluxes would respectively drive similar POC export fluxes at stations with high and low nutrient inventories remains to be determined.

4.2 POC/^{234}Th ratio and ^{234}Th-derived POC fluxes in the SCS basin

4.2.1 Variability in bottle- and trap-derived POC/^{234}Th ratios

Determining POC/^{234}Th ratios on particles at the export horizons is essential for converting ^{234}Th fluxes to POC export fluxes. POC/^{234}Th ratios can, however, vary by 3 orders of magnitude between different regions, depths, seasons and even particle sizes (Buesseler et al., 2006; Puigcorbé et al., 2020). The variability in POC/^{234}Th is possibly due to the combined effect of particle generation, aggregation, remineralization and particulate ^{234}Th decay (Cai et al., 2006). As shown in Fig. 7a, water column POC/^{234}Th ratios decreased gradually with depth and varied within 5 µmol dpm^{-1} below 50 m. This decreasing tendency of POC/^{234}Th ratios was highly consistent with results from prior studies conducted in tropical–subtropical oligotrophic ecosystems despite differing sampling devices (Puigcorbé et al., 2020). The maximum ratio with the highest variability was observed in the upper 25 m, at a depth where primary production usually peaks in oligotrophic ecosystems (Xie et al., 2018; Buesseler et al., 2020b). Even though POC/^{234}Th ratios determined from bottle filtration were variable in prior studies, they are strongly coupled to ratios from sediment traps (Gustafsson et al., 2013), which are considered to represent the ratio on sinking particles. POC/^{234}Th ratios based on bottle filtration and sediment traps in this study were also compared to each other at the same depth at station SEATS. The POC/^{234}Th ratios were 4.2 and 3.2 µmol dpm^{-1} on trap sam-

ples at 50 and 100 m, similarly to bottle-filtration-derived POC/^{234}Th ratios (4.4 ± 0.6 and 3.8 ± 0.6 µmol dpm^{-1} at 55 and 100 m, respectively). Besides bottle- and trap-derived POC/^{234}Th ratios, the POC/^{234}Th ratio on large-sized particles (> 53 µm and assumed to be sinking particles; Buesseler et al., 2006) retrieved from in situ pumping also decreased with depth at station SEATS (Cai et al., 2006) and converged to a narrow range from 1.8 to 4.1 µmol dpm^{-1} at 100 m in the SCS basin (Chen, 2008). We thus confirmed that the bottle-derived POC/^{234}Th was comparable with those derived from sinking particles accessed from traps or in situ pumps. This is consistent with prior studies showing that POC export fluxes based on bottle POC/^{234}Th were comparable with trap POC fluxes (e.g., Zhou et al., 2020a). Due to a lack of trap or pump deployment at all sites, and considering the similarity of POC/^{234}Th ratios using different methodologies, POC/^{234}Th ratios based on bottle filtration were used for POC flux estimation.

POC/^{234}Th ratios at the Ez base varied from 2.8 ± 0.4 to 8.3 ± 0.7 µmol dpm^{-1} (averaged at 4.2 ± 1.6 µmol dpm^{-1}; Fig. 7b), which is comparable with previously published results (e.g., 1.6 to 5.3 µmol dpm^{-1}, averaged at 4.2 ± 1.6 µmol dpm^{-1}) from the SCS basin (Cai et al., 2015; Zhou et al., 2013, 2020a). POC/^{234}Th ratios at the NDL base were generally higher than those at the Ez base, ranging from 3.2 ± 0.4 to 8.2 ± 1.1 µmol dpm^{-1} (averaged at 5.1 ± 1.7 µmol dpm^{-1}).

We found that variability in POC/^{234}Th ratios was insignificant between stations with shallow and deep nutriclines. The POC/^{234}Th ratio at the NDL base ranged from 4.4 ± 0.6 to 7.1 ± 0.9, averaged at 6.0 ± 1.0 µmol dpm^{-1} at stations with shallow nutriclines (i.e., stations SEATS, C1, A1 and A2), which was slightly higher than the values at other sites (ranging from 3.2 ± 0.4 to 8.2 ± 1.1, averaged at 4.5 ± 1.7 µmol dpm^{-1}). On the other hand, the

POC/^{234}Th ratios at the Ez base ranged from 2.9 ± 0.4 to 5.5 ± 0.7, averaged at $4.0 \pm 1.3 \, \mu\text{mol dpm}^{-1}$ at stations with shallow nutriclines, which was like the POC/^{234}Th ratios at other sites (ranging from 2.8 ± 0.4 to 8.3 ± 1.1, averaged at $4.3 \pm 1.7 \, \mu\text{mol dpm}^{-1}$). The relatively low POC/^{234}Th at the NDL base at stations with deep nutriclines may be explained by higher particle remineralization rates with increasing depth. Based on similar ranges of ^{234}Th fluxes and POC/^{234}Th ratios, the estimated POC export fluxes in this study were consistent with prior studies in the SCS basin (Cai et al., 2015; Zhou et al., 2020a).

4.2.2 POC export fluxes at different export horizons

POC export fluxes were estimated after combining the partitioned ^{234}Th fluxes and POC/^{234}Th ratios. ^{234}Th-derived POC export fluxes ranged from 1.2 ± 0.5 to $3.0 \pm 0.8 \, \text{mmol C m}^{-2} \, \text{d}^{-1}$ at the base of the Ez and from 1.2 ± 0.6 to $4.3 \pm 1.2 \, \text{mmol C m}^{-2} \, \text{d}^{-1}$ at the base of the NDL (Fig. 4e and Table 2). POC export fluxes estimated in this study are of the same order of magnitude as previous estimates in the SCS basin (Zhou et al., 2013, 2020a; Cai et al., 2015).

To assess the POC export flux using different methods, we compared ^{234}Th- and trap-derived POC export fluxes at station SEATS. POC export fluxes were comparable near the Ez base (2.9 ± 0.9 and $2.7 \pm 0.3 \, \text{mmol C m}^{-2} \, \text{d}^{-1}$ for ^{234}Th- and trap-derived POC export fluxes, respectively). However, the ^{234}Th-derived POC export flux of $1.6 \pm 0.6 \, \text{mmol C m}^{-2} \, \text{d}^{-1}$ was slightly lower than the trap-derived POC export flux ($2.8 \pm 0.3 \, \text{mmol C m}^{-2} \, \text{d}^{-1}$) at 50 m at station SEATS. The lower ^{234}Th-derived POC export flux at 50 m may indicate potential contamination by organics in the traps (e.g., swimmers) that would result in higher measured POC fluxes in the oligotrophic SCS basin. A recent study of the EXPORTS program found that swimmers could increase the measured POC export flux by a factor of 2 in the traps (Estapa et al., 2021). Although slight disagreement between different methods was often noted and difficult to assign causes (Hung and Gong, 2007; Stewart et al., 2007; Lampitt et al., 2008; Haskell et al., 2013; Buesseler et al., 2020b), we clearly found substantial POC export fluxes at the NDL base that were comparable to those at the Ez base in the SCS. A recent study based on ^{234}Th and sediment traps in the oligotrophic Gulf of Mexico also found particle production dominates in the upper Ez (0–60 m), where nutrients are depleted (Stukel et al., 2022). The results above conflict with previous knowledge suggesting that POC export flux from the nutrient-depleted mixed layer is extremely low (Coale and Bruland, 1987). The substantial POC export flux at the NDL base was highly correlated to the Chl a inventory, an index of biomass in the corresponding layer (Fig. 8a). In this regard, the sources of new nutrients that support the relatively high biomass in the NDL and drive the POC export fluxes at the NDL base in the SCS basin need to be constrained.

4.3 Diagnosis of nutrient sources supporting particle export in the oligotrophic SCS

4.3.1 Correlation between POC export flux and subsurface nutrient concentrations

To diagnose the nutrient sources that support POC export fluxes at different export horizons, we examined the relationship between partitioned POC export fluxes and nutrient inventories in corresponding layers. Nutrient stocks might regulate POC export fluxes at the Ez base based on their positive correlation (Fig. 8b, c). However, a poor relationship between POC export fluxes at the NDL base and nutrient inventories in the NDL was found, which suggests that the in situ nutrients in the NDL interior are insufficient to support the POC export from this horizon.

Other external nutrient sources must thus influence POC export flux in the nutrient-deleted ecosystems. Episodic events (e.g., eddies and typhoons) that can transport subsurface nutrients into nutrient-deficient regimes have been confirmed in other oligotrophic ocean regions (Johnson et al., 2010; Zhou et al., 2020b). Mesoscale eddies can pump subsurface nutrient-rich waters into the upper Ez and enhance surface Chl a based on a long-term dataset of the Chl a anomaly corresponding to eddy properties (e.g., SLA, amplitude and eddy rotation speed) in the oligotrophic SCS (He et al., 2016). Besides Chl a, POC concentrations and ^{234}Th deficits relative to ^{238}U were also significantly enhanced in the upper 25 m by impacts from cyclonic eddies in the oligotrophic SCS, where the nutrient concentrations were observed to be quite low (Zhou et al., 2020b). This enhancement of biomass would be amplified by the interplay of typhoons and cyclonic eddies (Liu et al., 2019). ^{15}N isotopic results also indicate that subsurface nitrate is an important external nutrient impacting export production (Yang et al., 2017). The nutrients from underlying waters may thus play an important role in supporting POC export from the NDL.

As the potential availability of subsurface nutrients was determined by the depth of the nutricline and the nutrient concentration in subsurface waters (Mouriño-Carballido et al., 2021), we examined relationships between partitioned POC export fluxes and the depth of the top of the nutricline and subsurface DIN and DIP concentrations below the Ez at 100, 125 and 150 m, where biological uptake might be negligible (Fig. 8d–j). The moderately positive correlation ($R^2 = 0.4$, $p < 0.05$) between the depth of the top of the nutricline and POC export fluxes at the NDL base (Fig. 8d) suggests that shallower nutriclines could indeed facilitate subsurface nutrient intrusion into the upper Ez and subsequently stimulate higher POC export fluxes in the upper nutrient-depleted ecosystems. Besides the nutricline, POC export fluxes at the NDL base were also correlated ($R^2 \geq 0.4$) with DIN and DIP concentrations in the subsurface water near or below the Ez base (Fig. 8e–j). The positive relationship thus suggests that POC export fluxes in the upper nutrient-depleted Ez are also
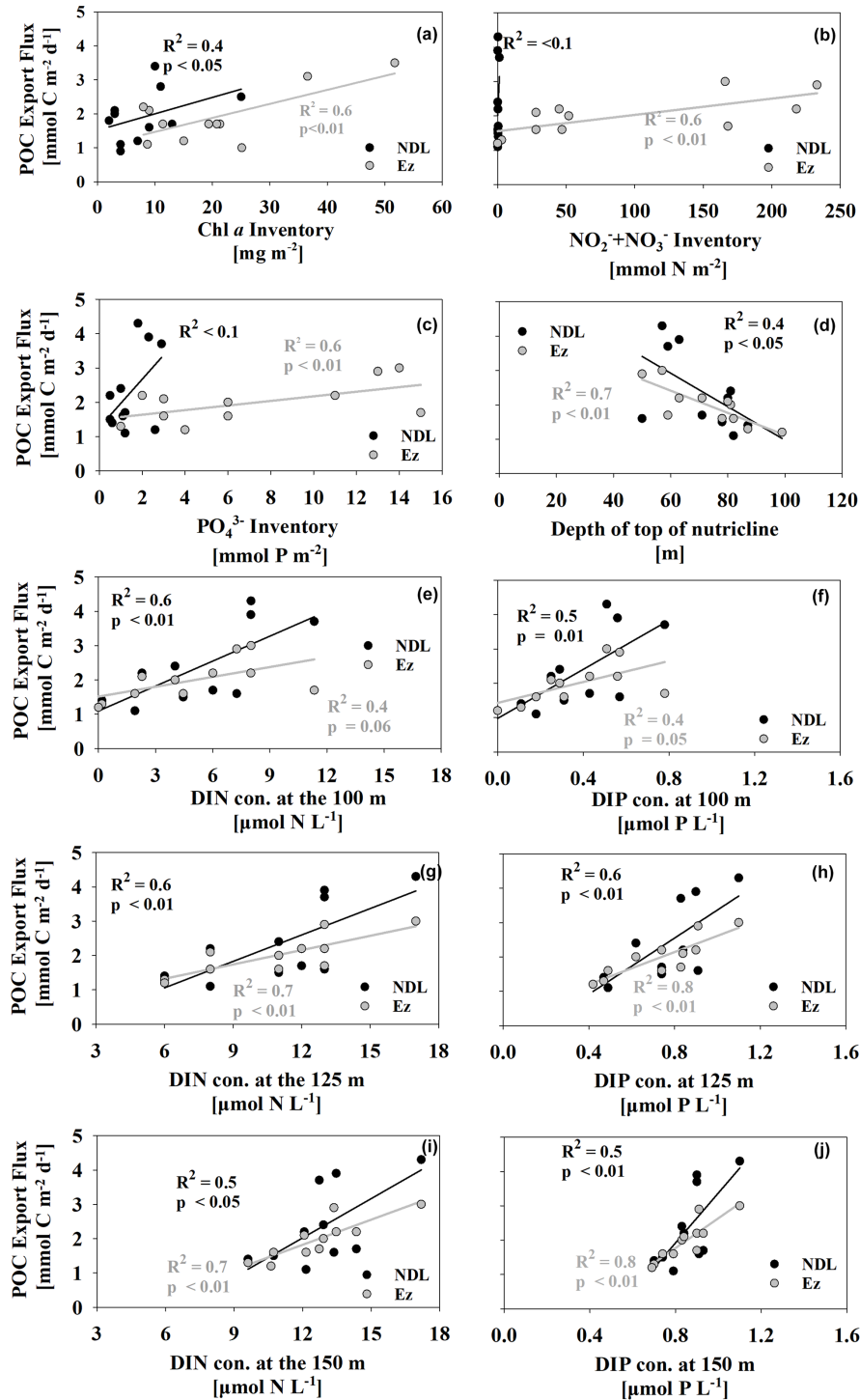
Figure 8. Relationship between POC export flux at the NDL base (black dots) and Ez base (gray dots) vs. Chl a **(a)**, DIN **(b)** and DIP inventories **(c)** in the corresponding layers. Also plotted are the relationships between the depth of the top of the nutricline **(d)** and DIN and DIP concentrations in subsurface water at 100, 125 and 150 m versus partitioning POC export fluxes **(e–j)**.

highly associated with subsurface nutrient levels. It is also noteworthy that the timescale of ship-based nutrients data is instantaneous, which may differ from the timescale of the ^{234}Th method (weeks to months). Consequently, the correlations between in situ nutrients and ^{234}Th-derived POC fluxes may be misinterpreted by the difference in timescales. To further investigate the correlations between nutrients and ^{234}Th-derived POC fluxes, ^{234}Th-derived POC fluxes were also related to the model-derived monthly average of nutrients (i.e., DIN concentration and the depth of nutricline; Du et al., 2021) during summer (Fig. S5 in the Supplement). The correlations between the two parameters were shown to be statistically significant ($P < 0.05$), again implying the importance of nutrient modulation to export fluxes.

4.3.2 Nutrient sources diagnosed via ^{15}N isotopic mass balance

As the timescale of ^{234}Th–^{238}U disequilibrium was not instantaneous, any episodic intrusion events before sampling (~ 20 d) could be recorded. Due to the limited Kuroshio intrusion into the SCS basin during the summer and the extremely low levels of nutrients in the surface Kuroshio current (Du et al., 2013), the lateral transport of nutrients by Kuroshio could be neglected over the study area. Thus, we assume that air-derived nitrogen (i.e., nitrogen fixation and atmospheric nitrogen deposition) and upwelled nitrate are the major sources of new N supporting PN-corresponding POC export out of the NDL and at the Ez base. Using a two-endmember mixing model based on the ^{15}N isotopic balance (Kao et al., 2012; Böttjer et al., 2017), we can evaluate the relative contribution of these two plausible sources of new N to support the particle export at sites SEATS and SS1 using the following equations:

$$1 = f_{NO_3^-} + f_{Air}, \tag{10}$$

$$\delta^{15}N_{PN} = \delta^{15}N_{NO_3^-} \times f_{NO_3^-} + \delta^{15}N_{air} \times f_{air}, \tag{11}$$

where $f_{NO_3^-}$ and f_{Air} represent the fraction of PN export contributed by upwelled DIN from the subsurface and by air-derived nitrogen from nitrogen fixation and atmospheric nitrogen deposition, respectively. $\delta^{15}N_{NO_3^-}$ and $\delta^{15}N_{air}$ denote the endmembers of $\delta^{15}N$ for subsurface DIN and air-derived N, respectively. $\delta^{15}N_{Air}$ is chosen as $-1.1\,‰$ by considering the influences of both nitrogen fixation and atmospheric nitrogen deposition following Yang et al. (2022). The $\delta^{15}N_{NO_3^-}$ values of subsurface DIN in the SCS basin are found to be unchanged spatially and temporally, with an average of $4.7 \pm 0.4\,‰$ at 100 m (Yang et al., 2017, 2022).

$f_{NO_3^-}$ was estimated to be about 59 %–67 % at the NDL base and 86 %–98 % at the Ez base at station SEATS. The proportion was higher (84 %–96 %) at 50 m within the NDL and nearly 100 % at 100 m close to the Ez base at station SS1. The differences in $\delta^{15}N_{PN}$ in the NDL are likely related to the

relative contributions of nutrient sources. Little variability in the regional nitrogen fixation rate suggests that differences in nitrogen fixation would not lead to such a discrete pattern of $\delta^{15}N_{PN}$ near the NDL base between sites, except when influenced by Kuroshio waters (Lu et al., 2018). However, Gao et al. (2020) clarified the spatial variation of atmospheric nitrogen deposition in the SCS basin, showing that the aerosol NO_3^- concentration at station SEATS was nearly twice that at station SS1, which is relatively far away from the continent. In addition, three anti-cyclonic eddies (Fig. S6 in the Supplement) influenced the water surrounding station SS1 before our visit in this region. In this regard, the relatively elevated contribution of subsurface DIN at station SS1 might be attributed to the decrease in atmospheric nitrogen deposition and event-driven subsurface DIN intrusion. Despite the variability of $\delta^{15}N_{PN}$ between stations, our results suggested a major contribution of subsurface DIN in the SCS basin based on the isotopic balance. These estimates indicate that POC export fluxes supported by subsurface DIN are sufficient and even more important than those supported by nitrogen fixation and atmospheric nitrogen deposition at the base of the NDL, where the DIN concentration is usually below detection. To validate our ^{15}N-based estimates, we compared the reported fluxes of nitrogen fixation and atmospheric nitrogen deposition in the SCS basin to the measured PN fluxes from the sediment trap at 50 m (about 2.8 mmol C m^{-2} d^{-1} and 0.42 mmol N m^{-2} d^{-1}, assuming a C/N ratio of 6.6 in sinking particles) at station SEATS in this study. The average nitrogen fixation rate was 0.06 mmol N m^{-2} d^{-1} (Kao et al., 2012; Chen et al., 2014), and the atmospheric nitrogen deposition flux was 0.14 mmol N m^{-2} d^{-1} (Yang et al., 2014; Kim et al., 2014). The contribution of nitrogen fixation and atmospheric nitrogen deposition to the measured PN flux at 50 m is estimated to be 48 %, suggesting that 52 % of PN flux at this depth is supported by subsurface nitrate. The derived $f_{NO_3^-}$ based on mass balance is slightly lower than that obtained from the isotopic balance at the NDL base (59 %–67 %). This might be due to an overestimation of the nitrogen fixation rate and the flux of atmospheric nitrogen deposition in the mass balance model. For example, the nitrogen fixation rate used is observed in the northeastern SCS, where the Kuroshio intrudes frequently (Kao et al., 2012). Higher rates of nitrogen fixation were detected in the Kuroshio-influenced waters compared to those in the northern basin (e.g., at station SEATS; Lu et al., 2019). Similarly, the observed flux of atmospheric nitrogen deposition at Dongsha Island, which is close to mainland China, is likely higher than that at station SEATS. Despite uncertainties, the two independent estimates both suggest a substantial role of subsurface nitrate in supporting particle export out of the NDL base. Furthermore, the differences in $\delta^{15}N_{PN}$ at both stations SEATS and SS1 gradually disappeared with increasing depth because the new nutrients were predominantly sourced from the nutrient-rich subsurface waters near the base of the Ez. This enhanced

contribution of subsurface nutrients is consistent with results from prior studies (Kao et al., 2012; Yang et al., 2017) that subsurface nutrients contribute to more than 90 % of the export production at the Ez base in the SCS basin.

Taken together, we thus hypothesize that the episodic event-driven nutrient upwelling from the subsurface to the surface nutrient-depleted ecosystem stimulates the growth of planktonic organisms and elevates the particle-scavenging rate in the oligotrophic SCS, which could be reflected in the ^{234}Th, whose activities integrate the impacts of processes occurring over several months. It is also worthwhile considering the influences of mesoscale and sub-mesoscale processes in the SCS basin. Prior studies showed the concurrence of the vertical transport of particles supported by locally uplifted nutrients and the horizontal transport of particles supported by the nutrients trapped in eddies (Wang et al., 2018; Ma et al., 2021). In this study, we found enhanced POC export fluxes at stations with high nutrient inventories and inferred that the POC export fluxes might also be supported by nutrients from the subsurface waters based on the signal of $\delta^{15}N_{PN}$. However, our current study was unable to diagnose the pathways of nutrients fueling the primary and export production, which need further studies.

5   Conclusions

With the aid of high-depth-resolution ^{234}Th sampling, ^{234}Th and POC fluxes at both the NDL and Ez bases were estimated in the oligotrophic SCS basin during the summer of 2017. Although DIN was exhausted in the NDL, ^{234}Th-based POC export fluxes at the NDL base were estimated to be 1.1 ± 0.5 to 4.3 ± 1.2 mmol C m^{-2} d^{-1}, which is comparable to those at the Ez base (1.2 ± 0.5 to 3.0 ± 0.8 mmol C m^{-2} d^{-1}). The relationship between POC export flux and nutrients was diagnosed: spatially, the POC export flux at the Ez base was elevated at stations with shallow nutriclines, corresponding to high nutrient inventories (1.7 ± 0.4 to 3.0 ± 0.8 mmol C m^{-2} d^{-1}) relative to stations with low nutrient inventories (1.2 ± 0.5 to 2.2 ± 1.2 mmol C m^{-2} d^{-1}). More than 50 % of the relatively high particle export occurring at the NDL base was verified by N isotopes to be supported by DIN from the subsurface. It thus indicated that other pathways (e.g., episodic events) might be important for nutrient intrusion into the Ez. The higher POC export flux resulted from shallow-nutricline-derived higher-nutrient stocks and biomass in the Ez. We thus hypothesize that subsurface nutrients might act as the primary regulator of POC export fluxes at both the Ez and NDL bases on a seasonal timescale. The reduced export flux against the background of higher surface temperature and stronger stratification further implies that sea surface warming might lower the efficiency of the BCP.

Author contributions. All authors were involved in the writing of the paper and approved the final submitted paper. YM and MD were major contributors to the study's conception, data analysis and drafting of the paper. KZ, WC and JC contributed significantly to cruise design, sample collections and/or data acquisition. JYTY contributed substantially to isotopic data acquisition and analysis.

References

Benitez-Nelson, C. R., Buesseler, K. O., and Crossin, G.: Upper ocean carbon export, horizontal transport, and vertical eddy diffusivity in the southwestern Gulf of Maine, Cont. Shelf Res., 20, 707–736, https://doi.org/10.1016/S0278-4343(99)00093-X, 2000.

Benitez-Nelson, C. R., Buesseler, K. O., Van Der Loeff, M., Andrews, J., Ball, L., Crossin, G., and Charette, M.: Testing a new small-volume technique for determining ^{234}Th in seawater, J. Radioanal. Nucl. Ch., 248, 795–799, https://doi.org/10.1023/a:1010621618652, 2001.

Böttjer, D., Dore, J. E., Karl, D. M., Letelier, R. M., Mahaffey, C., Wilson, S. T., Zehr, J., and Church, M. J.: Temporal variability of nitrogen fixation and particulate nitrogen export at Station ALOHA, Limnol. Oceanogr., 62, 200–216, https://doi.org/10.1002/lno.10386, 2017.

Buesseler, K. O., Bacon, M. P., Cochran, J. K., and Livingston, H. D.: Carbon and nitrogen export during the JGOFS North Atlantic Bloom experiment estimated from ^{234}Th : ^{238}U disequilibria, Deep-Sea Res. Pt. I, 39, 1115–1137, https://doi.org/10.1016/0198-0149(92)90060-7, 1992.

Buesseler, K. O., Benitez-Nelson, C. R., Moran, S., Burd, A., Charette, M., Cochran, J. K., Coppola, L., Fisher, N., Fowler, S., and Gardner, W.: An assessment of particulate organic carbon to thorium-234 ratios in the ocean and their impact on the application of ^{234}Th as a POC flux proxy, Mar. Chem., 100, 213–233, https://doi.org/10.1016/j.marchem.2005.10.013, 2006.

Buesseler, K. O., Pike, S., Maiti, K., Lamborg, C. H., Siegel, D. A., and Trull, T. W.: Thorium-234 as a tracer of spatial, temporal and vertical variability in particle flux in the North Pacific, Deep-Sea Res. Pt. I, 56, 1143–1167, https://doi.org/10.1016/j.dsr.2009.04.001, 2009.

Buesseler, K. O., Boyd, P. W., Black, E. E., and Siegel, D. A.: Metrics that matter for assessing the ocean biological carbon pump, P. Natl. Acad. Sci. USA, 117, 201918114, https://doi.org/10.1073/pnas.1918114117, 2020a.

Buesseler, K. O., Benitez-Nelson, C. R., Roca-Martí, M., Wyatt, A. M., Resplandy, L., Clevenger, S. J., Drysdale, J. A., Estapa, M. L., Pike, S., and Umhau, B. P.: High-resolution spatial and temporal measurements of particulate organic carbon flux using thorium-234 in the northeast Pacific Ocean during the EXport Processes in the Ocean from RemoTe Sensing field campaign, Elementa, 8, 30, https://doi.org/10.1525/elementa.2020.030, 2020b.

Cai, P., Dai, M., Chen, W., Tang, T., and Zhou, K.: On the importance of the decay of ^{234}Th in determining size-fractionated C/^{234}Th ratio on marine particles, Geophys. Res. Lett., 33, L23602, https://doi.org/10.1029/2006GL027792, 2006.

Cai, P., Chen, W., Dai, M., Wan, Z., Wang, D., Li, Q., Tang, T., and Lv, D.: A high-resolution study of particle export in the southern South China Sea based on ^{234}Th : ^{238}U disequilibrium, J. Geophys. Res.-Oceans, 113, C04019, https://doi.org/10.1029/2007JC004268, 2008.

Cai, P., Zhao, D., Wang, L., Huang, B., and Dai, M.: Role of particle stock and phytoplankton community structure in regulating particulate organic carbon export in a large marginal sea, J. Geophys. Res.-Oceans, 120, 2063–2095, https://doi.org/10.1002/2014JC010432, 2015.

Ceballos-Romero, E., Buesseler, K. O., and Villa-Alfageme, M.: Revisiting five decades of ^{234}Th data: a comprehensive global oceanic compilation, Earth Syst. Sci. Data, 14, 2639–2679, https://doi.org/10.5194/essd-14-2639-2022, 2022.

Chen, W. F.: On the export fluxes, seasonality and controls of particulate organic carbon in the Northern South China Sea, Ph.D. thesis, Xiamen University, China, 152 pp., 2008

Chen, Y.-L. L., Chen, H.-Y., Lin, Y.-H., Yong, T.-C., Taniuchi, Y., and Tuo, S.-H.: The relative contributions of unicellular and filamentous diazotrophs to N_2 fixation in the South China Sea and the upstream Kuroshio, Deep-Sea Res. Pt. I, 85, 56–71, https://doi.org/10.1016/j.dsr.2013.11.006, 2014.

Coale, K. H. and Bruland, K. W.: Oceanic stratified euphotic zone as elucidated by ^{234}Th : ^{238}U disequilibria, Limnol. Oceanogr., 32, 189–200, https://doi.org/10.4319/lo.1987.32.1.0189, 1987.

Cornec, M., Laxenaire, R., Speich, S., and Claustre, H.: Impact of mesoscale eddies on deep chlorophyll maxima, Geophys. Res. Lett., 48, e2021GL093470, https://doi.org/10.1029/2021GL093470, 2021.

Dore, J. E. and Karl, D. M.: Nitrite distributions and dynamics at Station ALOHA, Deep-Sea Res. Pt. II, 43, 385–402, https://doi.org/10.1016/0967-0645(95)00105-0, 1996.

Du, C., Liu, Z., Dai, M., Kao, S.-J., Cao, Z., Zhang, Y., Huang, T., Wang, L., and Li, Y.: Impact of the Kuroshio intrusion on the nutrient inventory in the upper northern South China Sea: insights from an isopycnal mixing model, Biogeosciences, 10, 6419–6432, https://doi.org/10.5194/bg-10-6419-2013, 2013.

Du, C., Liu, Z., Kao, S. J., and Dai, M.: Diapycnal Fluxes of Nutrients in an Oligotrophic Oceanic Regime: The South China Sea, Geophys. Res. Lett., 44, 11510–11518, https://doi.org/10.1002/2017GL074921, 2017.

Du, C., He, R., Liu, Z., Huang, T., Wang, L., Yuan, Z., Xu, Y., Wang, Z., and Dai, M.: Climatology of nutrient distributions in the South China Sea based on a large data set derived from a new algorithm, Prog. Oceanogr., 195, 102586, https://doi.org/10.1016/j.pocean.2021.102586, 2021.

Eppley, R. W. and Peterson, B. J.: Particulate organic matter flux and planktonic new production in the deep ocean, Nature, 282, 677–680, https://doi.org/10.1038/282677a0, 1979.

Estapa, M., Buesseler, K., Durkin, C. A., Omand, M., Benitez-Nelson, C. R., Roca-Martí, M., Breves, E., Kelly, R., and Pike, S.: Biogenic sinking particle fluxes and sediment trap collection efficiency at Ocean Station Papa, Elementa, 9, 00122, https://doi.org/10.1525/elementa.2020.00122, 2021.

Gan, J., Liu, Z., and Liang, L.: Numerical modeling of intrinsically and extrinsically forced seasonal circulation in the China Seas: A kinematic study, J. Geophys. Res.-Oceans, 121, 4697–4715, https://doi.org/10.1002/2016JC011800, 2016.

Gao, Y., Wang, L., Guo, X., Xu, Y., and Luo, L.: Atmospheric wet and dry deposition of dissolved inorganic nitrogen to the South China Sea, Sci. China Earth Sci., 63, 1339–1352, https://doi.org/10.1007/s11430-019-9612-2, 2020.

Goldman, J. C.: Oceanic Nutrient Cycles, in: Flows of Energy and Materials in Marine Ecosystems: Theory and Practice, edited by: Fasham, M. J. R., Springer US, Boston, MA, 137–170, https://doi.org/10.1007/978-1-4757-0387-0_6, 1984

Gustafsson, Ö., Gelting, J., Andersson, P., Larsson, U., and Roos, P.: An assessment of upper ocean carbon and nitrogen export fluxes on the boreal continental shelf: A 3-year study in the

open Baltic Sea comparing sediment traps, 234Th proxy, nutrient, and oxygen budgets, Limnol. Oceanogr.-Meth., 11, 495–510, https://doi.org/10.4319/lom.2013.11.495, 2013.

Haskell II, W. Z., Berelson, W. M., Hammond, D. E., and Capone, D. G.: Particle sinking dynamics and POC fluxes in the Eastern Tropical South Pacific based on 234Th budgets and sediment trap deployments, Deep-Sea Res. Pt. I, 81, 1–13, https://doi.org/10.1016/j.dsr.2013.07.001, 2013.

He, Q., Zhan, H., Cai, S., and Li, Z.: Eddy effects on surface chlorophyll in the northern South China Sea: Mechanism investigation and temporal variability analysis, Deep-Sea Res. Pt. I, 112, 25–36, https://doi.org/10.1016/j.dsr.2016.03.004, 2016.

Hung, C. C. and Gong, G. C.: Export flux of POC in the main stream of the Kuroshio, Geophys. Res. Lett., 34, L18606, https://doi.org/10.1029/2007GL030236, 2007.

Johnson, K. S., Riser, S. C., and Karl, D. M.: Nitrate supply from deep to near-surface waters of the North Pacific subtropical gyre, Nature, 465, 1062–1065, https://doi.org/10.1038/nature09170, 2010.

Kao, S. J., Terence Yang, J. Y., Liu, K. K., Dai, M., Chou, W. C., Lin, H. L., and Ren, H.: Isotope constraints on particulate nitrogen source and dynamics in the upper water column of the oligotrophic South China Sea, Global Biogeochem. Cy., 26, GB2033, https://doi.org/10.1029/2011GB004091, 2012.

Kim, T. W., Lee, K., Duce, R., and Liss, P.: Impact of atmospheric nitrogen deposition on phytoplankton productivity in the South China Sea, Geophys. Res. Lett., 41, 3156–3162, https://doi.org/10.1002/2014GL059665, 2014.

Knap, A., Michaels, A., Close, A., Ducklow, H., and Dickson, A. J.: Protocols for the joint global ocean flux study (JGOFS) core measurements, Reprint of the IOC Manuals Guides No. 29, UNESCO, 19, https://doi.org/10.25607/OBP-1443, 1996.

Lampitt, R. S., Boorman, B., Lucas, M. L., Salter, I., Sanders, R., Saw, K., Seeyave, S., Thomalla, S. J., and Turnewitsch, R.: Particle export from the euphotic zone: Estimates using a novel drifting sediment trap, 234Th and new production, Deep-Sea Res. Pt. I, 55, 1484–1502, https://doi.org/10.1016/j.dsr.2008.07.002, 2008.

Liu, K.-K., Kao, S.-J., Wen, L.-S., and Chen, K.-L.: Carbon and nitrogen isotopic compositions of particulate organic matter and biogeochemical processes in the eutrophic Danshuei Estuary in northern Taiwan, Sci. Total Environ., 382, 103–120, https://doi.org/10.1016/j.scitotenv.2007.04.019, 2007.

Liu, Y., Tang, D., and Evgeny, M.: Chlorophyll concentration response to the typhoon wind-pump induced upper ocean processes considering air–sea heat exchange, Remote Sens., 11, 1825–1847, https://doi.org/10.3390/rs11151825, 2019.

Liu, Z., Zhao, Y., Colin, C., Stattegger, K., Wiesner, M. G., Huh, C.-A., Zhang, Y., Li, X., Sompongchaiyakul, P., You, C.-F., Huang, C.-Y., Liu, J. T., Siringan, F. P., Le, K. P., Sathiamurthy, E., Hantoro, W. S., Liu, J., Tuo, S., Zhao, S., Zhou, S., He, Z., Wang, Y., Bunsomboonsakul, S., and Li, Y.: Source-to-sink transport processes of fluvial sediments in the South China Sea, Earth-Sci. Rev., 153, 238–273, https://doi.org/10.1016/j.earscirev.2015.08.005, 2016.

Lu, Y., Wen, Z., Shi, D., Chen, M., Zhang, Y., Bonnet, S., Li, Y., Tian, J., and Kao, S.-J.: Effect of light on N₂ fixation and net nitrogen release of Trichodesmium in a field study, Biogeosciences, 15, 1–12, https://doi.org/10.5194/bg-15-1-2018, 2018.

Lu, Y. Y., Wen, Z. Z., Shi, D. L., Lin, W. F., Bonnet, S., Dai, M. H., and Kao, S. J.: Biogeography of N₂ fixation influenced by the western boundary current intrusion in the South China Sea, J. Geophys. Res.-Oceans, 124, 6983–6996, https://doi.org/10.1029/2018JC014781, 2019.

Ma, Y. F. and Dai, M. H.: Vertical distribution of total and particulate 234Th, particulate organic carbon (POC) and nutrients with their physical forcings (temperature, salinity, fluorescence-based Chl a), Science Data Bank [data set], https://doi.org/10.57760/sciencedb.02782, 2023.

Ma, W. T., Xiu, P., Chai, F., Ran, L. H., Wiesner, M. G., Xi, J. Y., Yan, Y. W., and Fredj, E.: Impact of mesoscale eddies on the source funnel of sediment trap measurements in the South China Sea, Prog. Oceanogr., 194, 102566, https://doi.org/10.1016/j.pocean.2021.102566, 2021.

Mouriño-Carballido, B., Otero Ferrer, J. L., Fernández Castro, B., Marañón, E., Blazquez Maseda, M., Aguiar-González, B., Chouciño, P., Graña, R., Moreira-Coello, V., and Villamaña, M.: Magnitude of nitrate turbulent diffusion in contrasting marine environments. Sci. Rep., 11, 1–16, https://doi.org/10.1038/s41598-021-97731-4, 2021.

Okubo, A.: Oceanic diffusion diagrams, Deep-Sea Res., 18, 789–802, https://doi.org/10.1016/0011-7471(71)90046-5, 1971.

Owens, S. A., Buesseler, K. O., and Sims, K.: Re-evaluating the 238U-salinity relationship in seawater: Implications for the 238U-234Th disequilibrium method, Mar. Chem., 127, 31–39, https://doi.org/10.1016/j.marchem.2011.07.005, 2011.

Puigcorbé, V., Masqué, P., and Le Moigne, F. A. C.: Global database of ratios of particulate organic carbon to thorium-234 in the ocean: improving estimates of the biological carbon pump, Earth Syst. Sci. Data, 12, 1267–1285, https://doi.org/10.5194/essd-12-1267-2020, 2020.

Resplandy, L., Martin, A. P., Le Moigne, F., Martin, P., Aquilina, A., Mémery, L., Lévy, M., and Sanders, R.: How does dynamical spatial variability impact 234Th-derived estimates of organic export?, Deep-Sea Res. Pt. I, 68, 24–45, https://doi.org/10.1016/j.dsr.2012.05.015, 2012.

Savoye, N., Benitez-Nelson, C., Burd, A. B., Cochran, J. K., Charette, M., Buesseler, K. O., Jackson, G. A., Roy-Barman, M., Schmidt, S., and Elskens, M.: 234Th sorption and export models in the water column: A review, Mar. Chem., 100, 234–249, https://doi.org/10.1016/j.marchem.2005.10.014, 2006.

Scharek, R., Tupas, L. M., and Karl, D. M.: Diatom fluxes to the deep sea in the oligotrophic North Pacific gyre at Station ALOHA, Mar. Ecol.-Prog. Ser., 182, 55–67, https://doi.org/10.3354/meps182055, 1999.

Siegel, D. A., Buesseler, K. O., Behrenfeld, M. J., Benitez-Nelson, C. R., Emmanuel, B., Brzezinski, M. A., Adrian, B., Carlson, C. A., D'Asaro, E. A., and Doney, S. C.: Prediction of the Export and Fate of Global Ocean Net Primary Production: The EXPORTS Science Plan, Front. Mar. Sci., 3, 22, https://doi.org/10.3389/fmars.2016.00022, 2016.

Siegel, D. A., Cetinić, I., Graff, J. R., Lee, C. M., Nelson, N., Perry, M. J., Ramos, I. S., Steinberg, D. K., Buesseler, K., and Hamme, R.: An operational overview of the EXport Processes in the Ocean from RemoTe Sensing (EXPORTS) Northeast Pacific field deployment, Elementa, 9, 00107, https://doi.org/10.3389/fmars.2016.00022, 2021.

Satellite observations: Global Ocean Gridded L 4 Sea Surface Heights And Derived Variables Reprocessed 1993 Ongoing, CMS [data set], https://doi.org/10.48670/moi-00148, 2020.

Stewart, G., Cochran, J., Miquel, J., Masqué, P., Szlosek, J., Baena, A. R., Fowler, S., Gasser, B., and Hirschberg, D.: Comparing POC export from ^{234}Th/^{238}U and ^{210}Po/^{210}Pb disequilibria with estimates from sediment traps in the northwest Mediterranean, Deep-Sea Res. Pt. I, 54, 1549–1570, https://doi.org/10.1016/j.dsr.2007.06.005, 2007.

Stukel, M. R., Kelly, T. B., Landry, M. R., Selph, K. E., and Swalethorp, R.: Sinking carbon, nitrogen, and pigment flux within and beneath the euphotic zone in the oligotrophic, open-ocean Gulf of Mexico, J. Plankton Res., 44, 711–727, https://doi.org/10.1093/plankt/fbab001, 2022.

Umhau, B. P., Benitez-Nelson, C. R., Close, H. G., Hannides, C. C., Motta, L., Popp, B. N., Blum, J. D., and Drazen, J. C.: Seasonal and spatial changes in carbon and nitrogen fluxes estimated using ^{234}Th : ^{238}U disequilibria in the North Pacific tropical and subtropical gyre, Mar. Chem., 217, 103705, https://doi.org/10.1016/j.marchem.2019.103705, 2019.

Wang, L., Huang, B. Q., Laws, E. A., Zhou, K. B., Liu, X., Xie, Y. Y., and Dai, M. H.: Anticyclonic Eddy Edge Effects on Phytoplankton Communities and Particle Export in the Northern South China Sea, J. Geophys. Res.-Oceans, 123, 7632–7650, https://doi.org/10.1029/2017jc013623, 2018.

Winn, C. D., Campbell, L., Christian, J. R., Letelier, R. M., Hebel, D. V., Dore, J. E., Fujieki, L., and Karl, D. M.: Seasonal variability in the phytoplankton community of the North Pacific Subtropical Gyre, Global Biogeochem. Cy., 9, 605–620, https://doi.org/10.1029/95GB02149, 1995.

Wu, J., Lee, Z., Xie, Y., Goes, J., and Huang, B.: Reconciling between optical and Biological determinants of the euphotic zone depth, J. Geophys. Res.-Oceans, 126, e2020JC016874, https://doi.org/10.1029/2020JC016874, 2021.

Xie, Y., Laws, E. A., Yang, L., and Huang, B.: Diel patterns of variable fluorescence and carbon fixation of picocyanobacteria *Prochlorococcus*-dominated phytoplankton in the South China Sea basin, Front. Microbiol., 9, 1589–1604, https://doi.org/10.3389/fmicb.2018.01589, 2018.

Yang, J.-Y. T., Hsu, S.-C., Dai, M. H., Hsiao, S. S.-Y., and Kao, S.-J.: Isotopic composition of water-soluble nitrate in bulk atmospheric deposition at Dongsha Island: sources and implications of external N supply to the northern South China Sea, Biogeosciences, 11, 1833–1846, https://doi.org/10.5194/bg-11-1833-2014, 2014.

Yang, J. Y. T., Kao, S. J., Dai, M., Yan, X., and Lin, H. L.: Examining N cycling in the northern South China Sea from N isotopic signals in nitrate and particulate phases, J. Geophys. Res.-Biogeo., 122, 2118–2136, https://doi.org/10.1002/2016JG003618, 2017.

Yang, J. Y. T., Tang, J. M., Kang, S., Dai, M., Kao, S. J., Yan, X., Xu, M. N., and Du, C.: Comparison of nitrate isotopes between the South China Sea and western North Pacific Ocean: Insights into biogeochemical signals and water exchange, J. Geophys. Res.-Oceans, 127, e2021JC018304, https://doi.org/10.1029/2021JC018304, 2022.

Zhou, K., Dai, M., Kao, S.-J., Wang, L., Xiu, P., Chai, F., Tian, J., and Liu, Y.: Apparent enhancement of ^{234}Th-based particle export associated with anticyclonic eddies, Earth Planet. Sc. Lett., 381, 198–209, https://doi.org/10.1016/j.epsl.2013.07.039, 2013.

Zhou, K., Dai, M., Maiti, K., Chen, W., and Xie, Y.: Impact of physical and biogeochemical forcing on particle export in the South China Sea, Prog. Oceanogr., 187, 102403, https://doi.org/10.1016/j.pocean.2020.102403, 2020a.

Zhou, K., Dai, M., Xiu, P., Wang, L., Hu, J., and Benitez-Nelson, C. R.: Transient enhancement and decoupling of carbon and opal export in cyclonic eddies, J. Geophys. Res.-Oceans, 125, e2020JC016372, https://doi.org/10.1029/2020JC016372, 2020b.